Neuron, Vol. 27, 371–383, August, 2000, Copyright ©2000 by Cell Press

# Receptive Field Microstructure and Dendritic Geometry of Retinal Ganglion Cells

**Solange P. Brown,* Shigang He,†§ and Richard H. Masland*†‡**
*Program in Neuroscience
Harvard Medical School
Boston, Massachusetts 02115
†Howard Hughes Medical Institute
Massachusetts General Hospital
Boston, Massachusetts 02114

## Summary

**We studied the fine spatial structure of the receptive fields of retinal ganglion cells and its relationship to the dendritic geometry of these cells. Cells from which recordings had been made were microinjected with Lucifer yellow, so that responses generated at precise locations within the receptive field center could be directly compared with that cell's dendritic structure. While many cells with small receptive fields had dome-shaped sensitivity profiles, the majority of large receptive fields were composed of multiple regions of high sensitivity. The density of dendritic branches at any one location did not predict the regions of high sensitivity. Instead, the interactions between a ganglion cell's dendritic tree and the local mosaic of bipolar cell axons seem to define the fine structure of the receptive field center.**

## Introduction

A model based on a difference of Gaussians has become the standard description of the spatial organization of the receptive fields of retinal ganglion cells (Rodieck, 1965). Models of this type, with a central peak of sensitivity falling off toward the periphery, have formed the basis of most thinking about how these receptive fields are used in higher visual processing (Enroth-Cugell and Robson, 1966; Derrington and Lennie, 1982; Linsenmeier et al., 1982; Enroth-Cugell et al., 1983; Dawis et al., 1984; Soodak, 1986; Enroth-Cugell and Freeman, 1987; Hawken and Parker, 1987). Although a dome-shaped function may describe the general envelope of the sensitivity profile of the receptive field, there have been suggestions that additional fine structure exists within the receptive field center (Hochstein and Shapley, 1976; Thibos and Levick, 1983; Soodak et al., 1991; Rowe and Cox, 1993; Rowe and Palmer, 1995; Chichilnisky and Baylor, 1999). Most of these previous experiments used whole-field gratings delivered via the natural optics of the animal's eye to map the receptive fields. In the present studies, we used rabbit retinas maintained in vitro to identify an individual ganglion cell, probe its receptive field with high resolution methods, and inject it with a fluorescent dye to examine its dendritic morphology.

One of our goals was simply to see whether or not the description of receptive field sensitivity as dome-shaped is accurate for a variety of retinal ganglion cell types. Although the sensitivity profiles of cells with small receptive fields were essentially dome shaped, we found that the majority of ganglion cells with larger receptive fields had several regions of high sensitivity within the receptive field center.

Having determined that the receptive fields of some ganglion cells differ from the standard description, our second goal was to visualize the anatomical substrate of the receptive field. Modeling studies have tried to predict an idealized receptive field from the structure of representative ganglion cells described independently (Koch et al., 1982; Cohen and Sterling, 1991; Freed et al., 1992; Kier et al., 1995). Others have used physiological data to theorize about the underlying dendritic structure (Creutzfeldt et al., 1970; Thibos and Levick, 1983; Soodak et al., 1991; Rowe and Cox, 1993; Rowe and Palmer, 1995). By injecting the cell with Lucifer yellow immediately after recording, we could compare a precisely measured receptive field with the dendritic arbor of the particular cell that generated it. The most striking inhomogeneities were found for the larger types of ganglion cell. We suggest a mechanistic reason why this might be so and why these irregularities would be an acceptable cost for an efficient overall plan of the visual system.

## Results

The basic technique used to map the receptive fields of retinal ganglion cells is illustrated in Figure 1. For each cell, we first calculated the spike-triggered average of the stimulus using the largest pixel size in our protocol, 104 μm (0.6° of visual angle). An example of such a spatiotemporal receptive field is shown in Figure 1A for an ON brisk transient cell (DeVries and Baylor, 1997). The mean effective stimulus in this case was a transition from OFF (red pixels in the frames from −156.2 to −99.4 ms prior to the action potential) to ON (green pixels from −99.4 to −42.6 ms prior to the action potential). For concentric retinal ganglion cells, the same pixels were consistently the most influential through different phases of the visual response; in other words, the spatial structure did not change in the different phases of the response. Therefore, we defined the spatial receptive field as the stimulus frame with the maximum modulation of the same sign (i.e., ON or OFF) as the cell's response to a simple spot (see Experimental Procedures). For the ON cell in Figure 1, this was the average stimulus that preceded the action potential by 71 ms (Figure 1B).

### Ganglion Cells Contain Hot Spots of Sensitivity within Their Receptive Fields

Figure 1B shows the cross section of the sensitivity profile of the receptive field center along two axes. Along

‡To whom correspondence should be addressed (e-mail: masland@helix.mgh.harvard.edu).
§Current address: Institute of Neuroscience, Chinese Academy of Sciences, 320 Yue-Yang Road, Shanghai 200031, China.

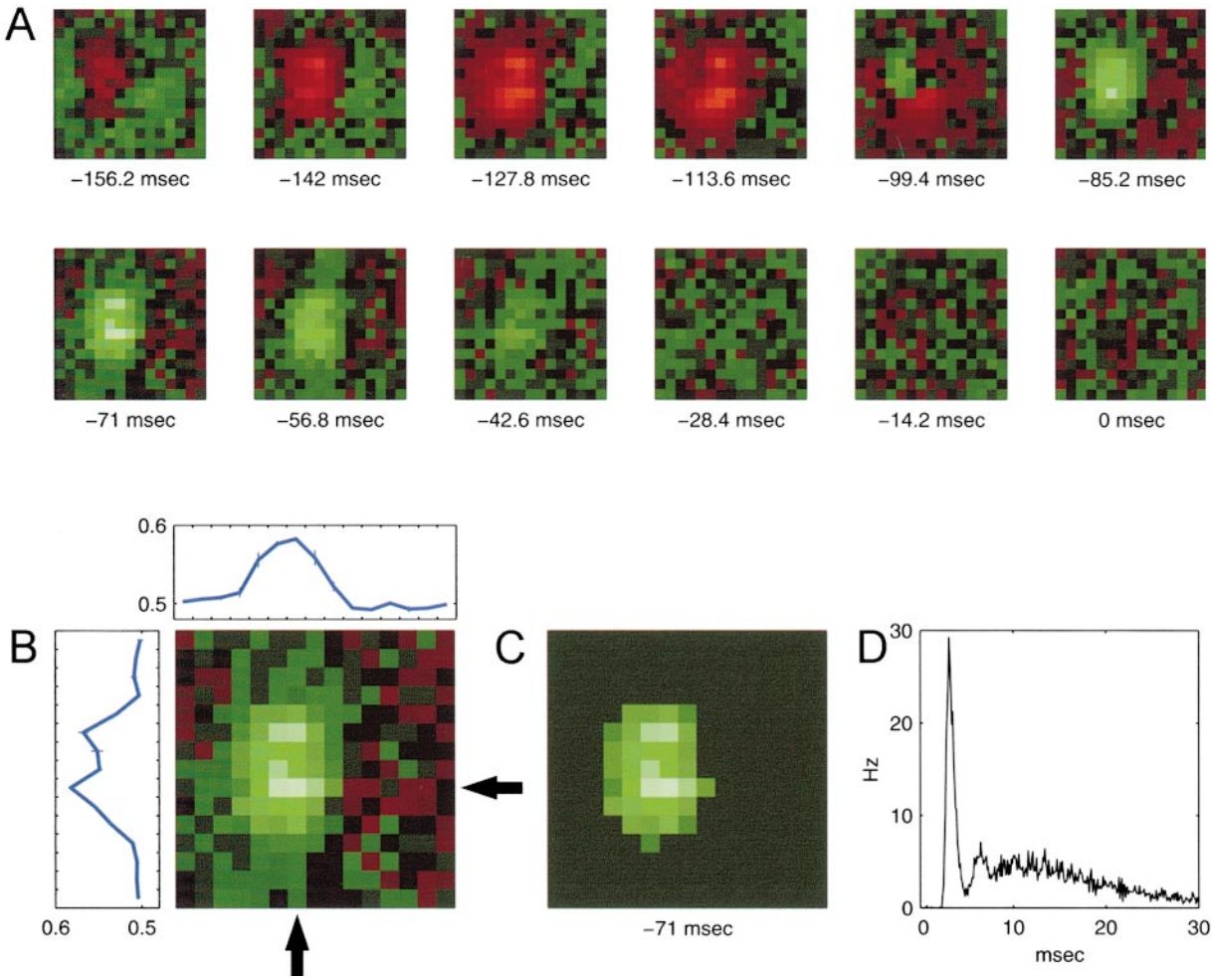


Figure 1. Method for Determining the Spatial Sensitivity Profile of the Receptive Field Center

Each cell was mapped using a stimulus of spatiotemporal white noise. The spike-triggered stimulus average was calculated for each cell, resulting in a movie of the mean effective stimulus preceding the action potential.

(A and B) A 150 ms segment from one movie is displayed with time moving from left to right and top to bottom. The action potential occurs at 0 delay (bottom right movie frame). The movie is shown in 14.2 ms steps preceding the onset of the action potential, with time indicated in ms under each frame (see Experimental Procedures). The red pixels indicate when and where the cell was excited by dark pixels of the stimulus (or inhibited by light pixels), while the green pixels indicate when and where the cell was excited by light pixels (or inhibited by dark pixels). This cell responds best to an OFF (red) to ON (green) transition in the stimulus, as would be expected from an ON-brisk transient cell (DeVries and Baylor, 1997). As this spatiotemporal receptive field illustrates, the positions of regions of high sensitivity do not change with time: compare the frames at −127.8 ms and −71 ms, the peak of the OFF and ON phases of the response, respectively. The maximum modulation of the polarity of the neuron's response to a spot occurred in the movie frame that preceded the action potential by 71 ms. This frame, shown in more detail in (B), shows the spatial configuration of the stimulus that, on average, most strongly affected the firing rate of the cell and represents the spatial receptive field of the cell (see Experimental Procedures). Two cross sections of the sensitivity profile are shown above and to the left of the receptive field. The plot above the receptive field represents the cross section of the sensitivity profile at the level of the arrowhead on the right. The sensitivity profile had a single peak in this orientation. The plot to the left of the receptive field represents the cross section of the sensitivity profile at the level of the arrowhead below the receptive field. In this orientation, the sensitivity profile clearly had two peaks. The error bars represent the standard errors of the mean for the four stimulus runs. The scale on the two axes represents the absolute stimulus intensity, with 0.5 indicating mean luminance and 0 and 1 the minimum and maximum intensity excursions, respectively.

(C) The stimulus frame shown in (B) has been thresholded to show only those pixels that were modulated more than three standard deviations from the mean (see Experimental Procedures). This criterion can be used to judge the spatial extent of the receptive field.

(D) The autocorrelogram for one stimulus run is shown. There is a clear refractory period, indicating that action potentials from only a single cell were analyzed.

In (A), (B), and (C), each square in the receptive field measures 104 μm.

one axis, from left to right, the cell has a smooth sensitivity profile with a single peak. However, along the axis from top to bottom, there are two peaks in the sensitivity profile. The peaks were reproducible across mapping runs; the error bars represent ±1 SEM.

Using these techniques, we mapped the receptive fields of 79 concentric cells and found a broad variety of sensitivity profiles for the receptive field center. Two examples are shown in Figure 2. The receptive field profiles formed a continuum from small and dome-shaped to elongated to quite irregular. Less than 40% of the cells in our sample had essentially dome-shaped

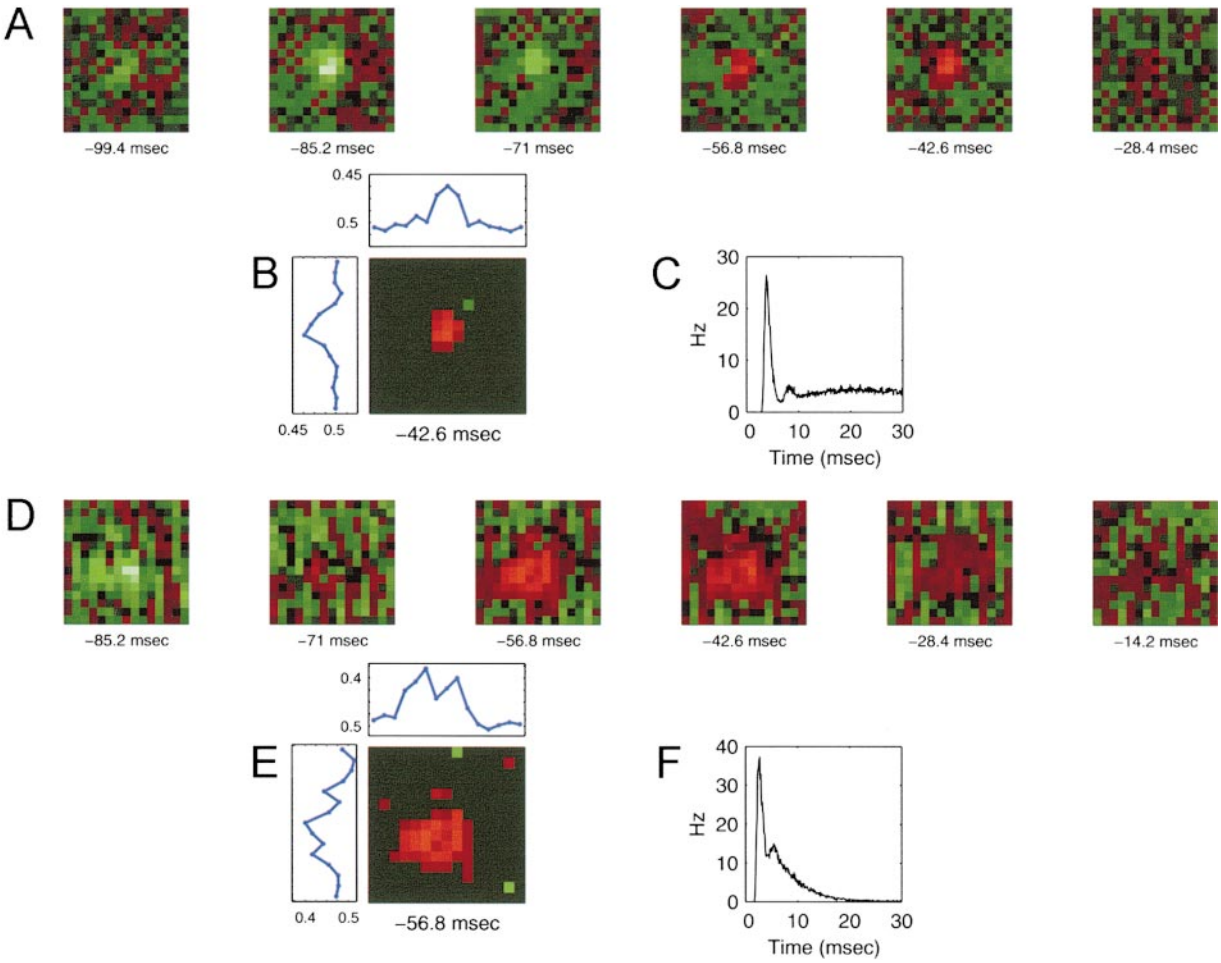


Figure 2. Examples of Receptive Fields

(A) This OFF cell had one of the largest dome-shaped receptive fields encountered. Six frames of the spatiotemporal receptive field are shown in succession to illustrate how the receptive field evolved over time. Each frame shows the average stimulus, which preceded the action potential by the delay in milliseconds noted below each frame. Time proceeds from left to right.

(B) The thresholded spatial receptive field of the cell in (A), 42.6 ms preceding the action potential. The two cross sections of the sensitivity profile are also shown above and to the left of the receptive field, highlighting its dome-shaped nature with a single region of high sensitivity.

(C) The autocorrelogram for the cell in (A).

(D) This OFF cell has a more irregular receptive field, with regions of high sensitivity and intervening regions of lower sensitivity.

(E) The thresholded receptive field is shown flanked by two cross sections of the cell's sensitivity profile.

(F) The autocorrelogram for the cell in (D).

In (A), (B), (D), and (E), each square in the receptive field measures 104 μm.

sensitivity profiles, as shown in Figure 2A. Most of these receptive fields were small, ranging from 100 to 400 μm in diameter. The cell shown had one of the largest such receptive fields in our sample.

Large receptive fields often were elongated or irregularly shaped and had more than one region of high sensitivity within their receptive fields. Cells with elongated receptive fields, like the one shown in Figure 1, had regions of high sensitivity flanking a less sensitive central region. Other, more irregular receptive fields were also encountered (Figure 2D). Six cells even had distinctly "C"-shaped receptive fields (see Figure 4). There was no relationship between the axis of elongation or the axis of the C shape and the position of the electrode. Optical interference from the electrode was unlikely in any case, since the stimulus was projected to the photoreceptor side of the retina, while the electrode approached from the ganglion cell side (see Experimental Procedures).

### The Inhomogeneities Were Not Due to Multicell Recording or Damage to the Retina

A trivial explanation for the multiple regions of high sensitivity within the receptive field would be that we were mistakenly recording from more than one ganglion cell. For example, the aggregate response of two symmetric receptive fields displaced from one another could very well look like the receptive field shown in Figure 1. However, the spike shapes and the autocorrelograms for each cell leave no doubt that action potentials from only a single cell were analyzed (Figures 1D, 2C, 2F, and 5F). Furthermore, some of the irregular cells in our sample were recorded using a loose patch technique; with this method, it is difficult to imagine that action potentials from more than one cell were recorded.

A second concern was that we had somehow damaged the photoreceptors during the isolation of the retina for in vitro recording. Some regions of the receptive field center might be less sensitive only because the

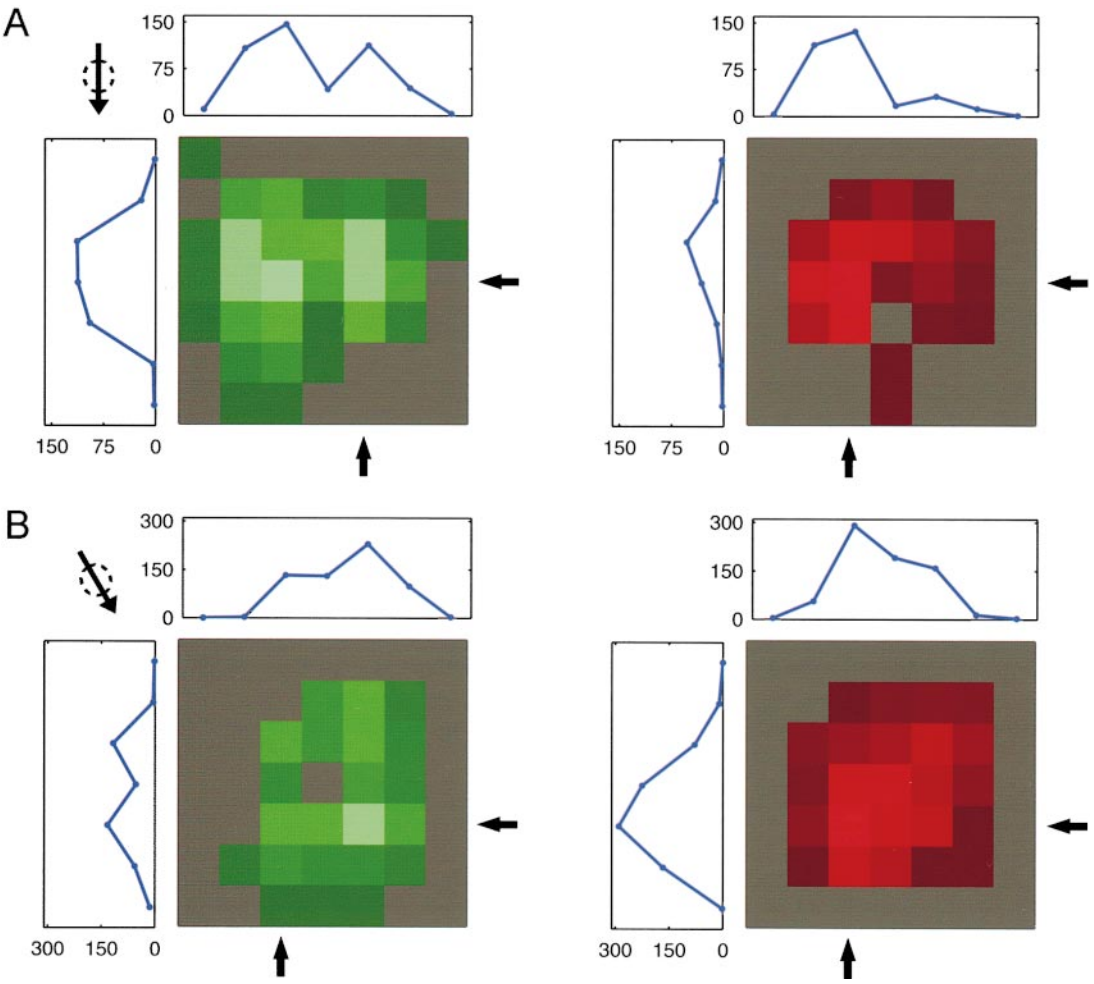


Figure 3. Comparison of the ON and OFF Receptive Fields for Two ON–OFF DS Ganglion Cells

(A) The responses to the onset (left) and offset (right) of the light of an ON–OFF DS cell is shown. Two cross sections of the sensitivity profile for each response are plotted above and to the left of the receptive field. In some regions of the receptive field, the maximum sensitivity of the cell's ON and OFF response is very similar (see left portion of the horizontal cross section). However, in other regions of the receptive field, the sensitivities of the two responses are markedly different, indicating that damage to the overlying photoreceptors was not artifactually generating the sensitivity profiles. The axes on the cross sections indicate the number of spikes elicited in the 500 ms following the onset or offset of the stimulus.

(B) An example from another ON–OFF DS cell is shown.

In (A) and (B), each square in the receptive field measures 100 μm. The preferred direction for each cell is shown in the upper left-hand corner of the ON receptive field.

photoreceptors in that region of the receptive field were damaged. However, when we examined the tissue, we did not identify anatomically any damaged regions that correlated with the variations in center sensitivity. Furthermore, we used a variety of recording configurations, including Ames-Pollen electrodes, blunt wires of platinum–iridium gently placed on the surface of the retina without breaking through the inner limiting membrane (Ames and Pollen, 1969), to decrease the likelihood of damaging the retina. We found no systematic differences in the receptive fields mapped using the different recording techniques. None of the features of the receptive fields, such as the axis of elongation, correlated with the type of electrode used or the direction from which it approached the cell.

We tested these conclusions functionally by taking advantage of the unique structure of ON–OFF direction-selective (DS) ganglion cells. These cells respond to both the onset and the offset of a stimulus. Correspondingly, they have bistratified dendritic arbors, with one arbor ramifying in the ON sublamina of the inner plexiform layer (IPL) and the other ramifying in the OFF sublamina of the IPL. Since the same photoreceptors provide input to the ON and OFF responses of these cells, the ON receptive field can provide a control for the structure in the OFF receptive field, and vice versa. If the overlying photoreceptors were damaged, sensitivity profiles of the ON and OFF receptive fields should be similar.

As with the concentric cells, a continuum of sensitivity profiles was encountered. A handful of ON–OFF DS cells with small receptive fields had ON and OFF receptive fields with essentially similar dome-shaped sensitivity profiles. However, the majority of the ON–OFF DS cells in our sample had different sensitivity profiles for the ON and OFF receptive fields. Examples of two such

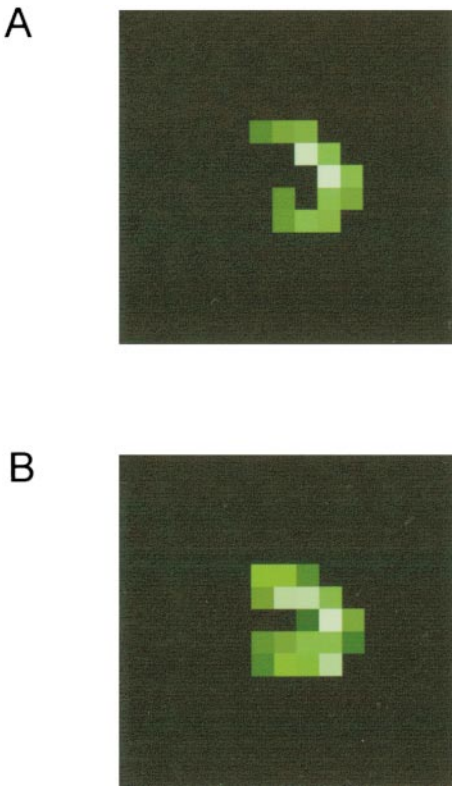


Figure 4. Comparison of the Spike-Triggered Stimulus Average and Traditional Spot Mapping

(A) The spike-triggered average of the cell 42.6 ms preceding the action potential. Only those pixels that were modulated more than three standard deviations from the mean are shown.

(B) The same cell was mapped using individual presentations of single spots of light. The same square size (104 μm) was used as in (A). Ten presentations of the 225 individual spots were randomly interleaved. Each trial consisted of light ON for 200 ms followed by 1.5 s of the dim background. Each pixel represents the number of spikes during the first 100 ms following light ON; the maximum spike rate was 51 Hz. The receptive field was thresholded at the level of the spontaneous activity. Despite the two different techniques used, the basic features of the receptive field were quite similar.

cells are shown in Figure 3. Note that the ON and OFF receptive fields had similar peak sensitivities but that the locations did not correlate with one another.

### Varying the Visual Stimulus Did Not Affect the Location of the Hot Spots

We compared the maps acquired using the spatiotemporal white noise stimulus with the traditional technique of mapping receptive fields with single spots of light. Figure 4 shows one such comparison for an ON cell. The spike-triggered stimulus average is shown in Figure 4A; it was calculated from ~7.5 min (32,000 video frames at ~70 Hz) of the checkerboard stimulus. In Figure 4B, we mapped the receptive field of the same cell by flashing each square of the checkerboard stimulus in isolation and counting the action potentials in the 100 ms following the stimulus onset. The presentation of the 225 individual squares was randomly interleaved in the ten trials. Each square was presented for 200 ms followed by 1.5 s of dim background; the entire protocol required ~73 min to complete. The two techniques revealed a similar C-shaped receptive field.

Would more structure be revealed when the receptive field center is mapped at a finer scale? The effect of varying the size of the squares used in the checkerboard pattern is shown in Figure 5. The cell was first mapped with 104 μm squares (Figure 5A), revealing two regions of high sensitivity within an oblong receptive field. Although the two regions of high sensitivity became increasingly distinct as the pixel size of the stimulus was reduced, the sensitivity profile of the cell did not qualitatively change with decreasing pixel size. Even at the smallest square size used—32 μm—there were still two regions of relatively high sensitivity that flanked a central region of decreased sensitivity within this oblong receptive field (Figure 5D). When the cross sections of the four different maps of the receptive field are superimposed, the striking similarity among them is evident (Figure 5E).

### The Hot Spots Are Not Predicted by the Position of the Soma or Dendrites of the Ganglion Cell

The spatiotemporal spike-triggered average of the cell's receptive field was measured using a square size of 104 μm, after which the cell was injected with Lucifer yellow to visualize its dendritic tree (Figure 6A). A photograph was immediately taken of the cell and a fiduciary mark projected from the stimulus monitor (Figure 6B). The soma could now be localized relative to the receptive field map (Figure 6C). The yellow spot placed on the receptive field in Figure 6C shows the position of the soma relative to the receptive field map. The position of the fiduciary mark in Figure 6B is outlined in yellow in Figure 6C.

We quantitatively compared the position of the soma, the center of mass of the receptive field, and the position of the most influential pixel of the spike-triggered stimulus average—the peak sensitivity—for 21 cells. For 3 cells, the locations of the soma, center of mass, and most influential pixel were the same. These cells had very small receptive fields. For the remaining cells, the pixel that most influenced the firing rate of the cell was situated at some distance from the soma. Figure 7A shows an example from one cell. The most influential pixel was displaced relative to the soma. The soma was located within a region of decreased sensitivity.

Figure 7B summarizes the data for all 21 cells examined in this way. The green circles represent the centers of mass of the 21 receptive fields. The red asterisks represent the locations of the most influential pixels relative to the somas of the cells. The most modulated pixel was, on average, located farther from the soma (mean, 176 μm) than was the center of mass of the receptive field center (mean, 114 μm) in this group of 21 cells ($p = 0.023$, two-tailed t test). When a similar analysis was performed for the second and third most influential pixels, the effect was even more pronounced. The average distance to the soma was 222 μm for the second most modulated pixel and 220 μm for the third most modulated pixel. All were significantly different from the mean distance of the center of mass to the soma (two-tailed t test, $p < 0.001$). These results indicate that, for large cells, the regions of high sensitivity are often offset from the position of the soma. These regions were as much as 30% more sensitive than was the region over the soma.

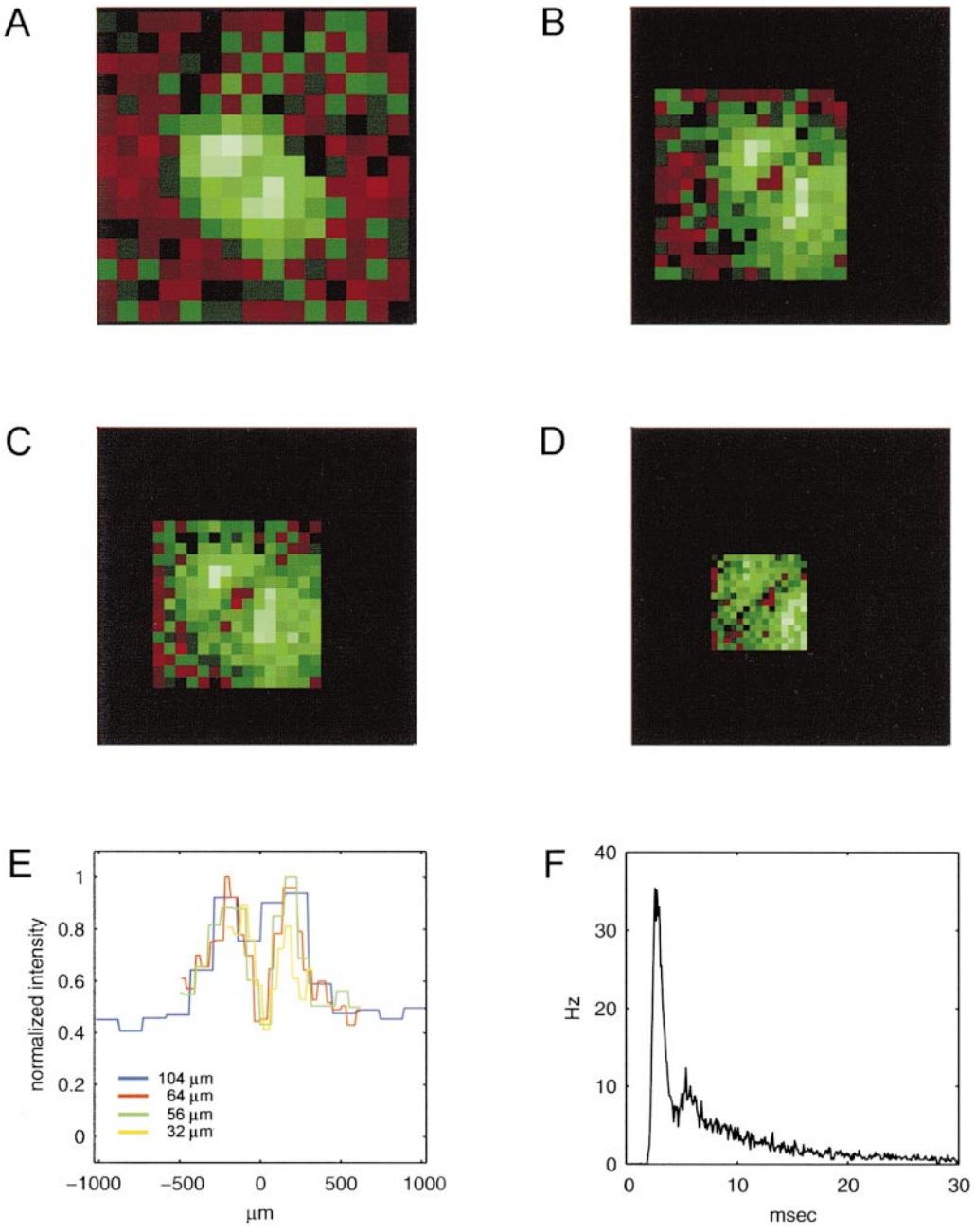


Figure 5. The Effect on the Sensitivity Profile of Mapping with Pixels of Different Sizes

(A) This ON cell was first mapped with the standard stimulus, consisting of 225 104 μm squares. Two regions of high sensitivity flanked a central region of relatively decreased sensitivity in this oblong receptive field.

(B) The spatial receptive field measured with 225 64 μm stimulus pixels. The receptive field was quite similar. At this finer scale, the two regions of high sensitivity were more clearly delineated.

(C) This receptive field map was generated using stimulus pixels 56 μm in width.

(D) The finest scale used to map the receptive field was a square size of 32 μm. For technical reasons, we were limited to 15 × 15 total pixels in the stimulus. Although the 225 squares did not fully cover the receptive field, the central region of decreased sensitivity was clearly preserved. No qualitative differences in the receptive field were revealed as compared with the receptive field map in (A).

(E) One cross section of the sensitivity profile from each of the four receptive field maps in (A) through (D) is plotted. The cross section was taken from the lower right to the upper left of the four maps of the receptive field. The basic features of the sensitivity profile are easily recognized in all four profiles.

(F) The autocorrelogram from the stimulus run in (A). The morphology of the cell is shown in Figure 8D.

In Figure 8, the dendritic morphology of four cells is shown relative to the sensitivity profiles of each cell's receptive field center. In all cases, the soma is located in a region of relatively decreased sensitivity. There are no gross asymmetries within the dendritic structure of these cells that can be used to predict the location of the regions of high sensitivity within the receptive field. Areas of reduced sensitivity do not simply represent

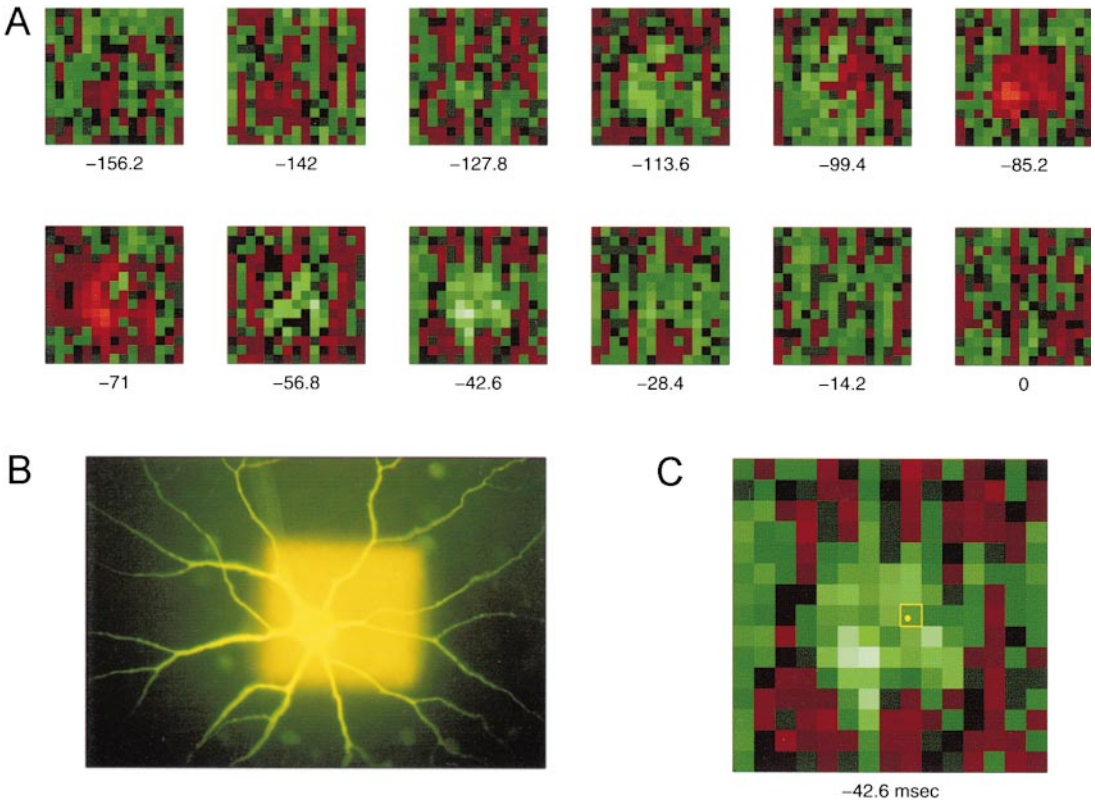


Figure 6. Technique for Aligning the Profile of the Receptive Field with the Morphology of Each Cell

(A) Each cell was first mapped using a spatiotemporal white noise stimulus with a square size of 104 μm. Twelve frames of the mean effective stimulus in 14.2 ms steps are shown. Time proceeds from left to right and top to bottom, spanning 156.2 to 0 ms preceding the action potential.

(B) The cell was injected with Lucifer yellow. A square, 104 μm across, was projected from the stimulus monitor. A photograph of the soma and proximal dendrites with this fiduciary mark was immediately taken. The white stimulus appears yellow because it was photographed through a filter set appropriate for viewing Lucifer yellow.

(C) The position of the soma of this cell has been superimposed on the receptive field of the cell. The yellow dot indicates the position of the soma. The 104 μm square in (B) is outlined in yellow. The morphology of this cell is shown in Figure 8B.

areas devoid of dendritic branches (as has been suggested; Creutzfeldt et al., 1970; Thibos and Levick, 1983; Rowe and Cox, 1993; Rowe and Palmer, 1995). As demonstrated above, mapping at finer detail did not reveal any additional relationship between the fine structure within the sensitivity profile of the cell and its dendritic morphology (compare Figure 8D and Figures 5A–5D). Generally, the pattern of dendritic branches varies on a much finer scale than do the sensitivity profiles of the cells.

## Discussion

The receptive fields of more than 60% of the retinal ganglion cells in our sample had a sensitivity profile far from the traditional smooth Gaussian, displaying an irregular, even C-shaped, footprint and two or more regions of high sensitivity. Irregular sensitivity profiles of individual cells were not due to optical aberrations, as the stimuli were delivered in vitro by a high quality optical system. When reverse correlated responses to flickering checkerboards were measured, the sensitivity profiles of individual cells were stable across different stimulus sequences. For individual cells, the same profiles were revealed by reverse correlation and forward mapping of stimulus-triggered responses to single spots.

The irregularities were not due to local damage to individual cells or the retina's overall structure: they were observed using the blunt, low-resistance Ames-Pollen electrodes, which do not penetrate the inner limiting membrane. More important, a class of bistratified ON–OFF cell that has two independent dendritic arbors showed independent hot spots at different locations for the ON and OFF responses. If the retina had been mechanically damaged—for example, by pressure on the photoreceptors—the resulting regions of low sensitivity should have been the same for both types of response. Finally, anisotropies in ganglion cell receptive fields have previously been detected using recordings made in vivo from the optic nerve or lateral geniculate nucleus (Hochstein and Shapley, 1976; Soodak et al., 1991). Although such methods relied on whole-field gratings to characterize the receptive fields, these findings once again show that irregular receptive fields are not a consequence of mechanical disturbance of the retina.

### Receptive Field Inhomogeneities May Originate from the Wide Spacing of Dendrites in Wide-Field Ganglion Cells

A number of theoretical studies have modeled the relationship between the pattern of ganglion cell dendrites

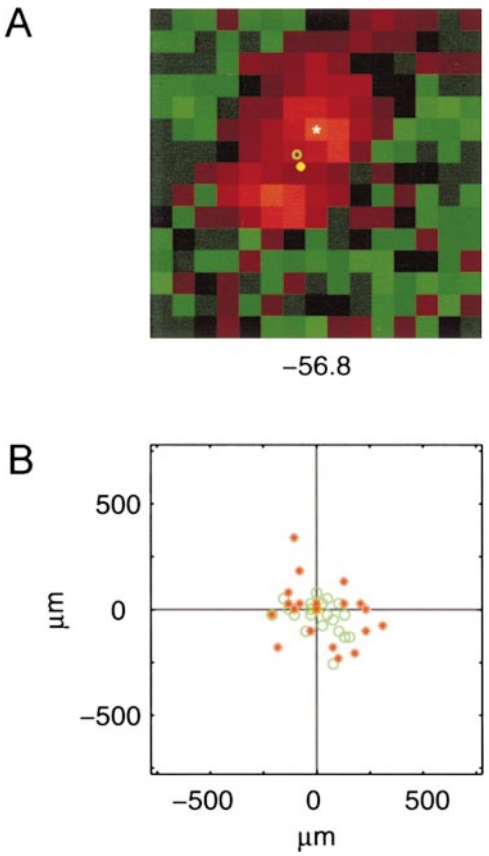


Figure 7. The Relationships among the Soma, the Center of Mass of the Receptive Field, and the Most Sensitive Region of the Receptive Field

(A) The receptive field of an OFF cell is shown. The yellow dot marks the position of the soma. The green circle marks the position of the center of mass of the receptive field. The white asterisk marks the most influential pixel of this OFF cell's receptive field.

(B) The positions of the centers of mass (green "o") and the most modulated pixels (red asterisk) relative to the somas of 21 different cells are plotted at the same spatial scale as in (A). The spatial coordinates were translated such that the position of each cell's soma is centered at the intersection of the black lines. All cells were mapped using squares 104 μm in width. For three cells, all with small receptive fields, the center of mass, the most modulated pixel, and the soma were all colocalized. In our sample, the center of mass of the receptive field was, on average, located closer to the soma than was the most influential pixel (114 μm versus 176 μm, $p = 0.023$, two-tailed t test).

and the physiological characteristics of the cell's receptive field. In the present study, the two can be directly compared.

Electrotonic models of the receptive field center generate the (canonical) domed sensitivity of the retinal ganglion cell via attenuation of distal synaptic inputs by the passive cable properties of the dendrites (Creutzfeldt et al., 1970; Koch et al., 1982). These models have been criticized previously for theoretical reasons (Freed et al., 1992; Velte and Miller, 1995) and are clearly incompatible with our observation that the largest cells in our sample—the most vulnerable to passive cable properties—often had a dip in sensitivity over the soma, whereas the models predict a peak in sensitivity.

A second class of models suggests that specific anatomical features generate the dome-shaped sensitivity profile. For example, the overall geometry of a ganglion cell's arbor may perfectly reflect the sensitivity profile of the cell, decreasing in density from center to periphery (Creutzfeldt et al., 1970; Kier et al., 1995). Alternatively, the specific distribution of bipolar cell synapses may weight these inputs to yield a dome-shaped sensitivity profile (Cohen and Sterling, 1991; Freed et al., 1992). These speculations are plausible and may be correct for the 40% of our cells—the small-field cells—that did have dome-shaped receptive fields. Neither can be correct for the 60% of our sample—almost entirely made up of wide-field cells—in which the profile of the receptive field deviated from the domed shape assumed by both previous analyses.

A third type of model proposes that the sensitivity profile is controlled by the detailed morphology of the ganglion cell's dendritic arbor. Regions of high sensitivity would correspond to those regions of the presynaptic bipolar cell array that are most densely sampled, in other words, those areas with the highest density of ganglion cell dendrites and/or their synapses with bipolar cells (Creutzfeldt et al., 1970; Thibos and Levick, 1983; Soodak et al., 1991; Rowe and Cox, 1993; Kier et al., 1995; Rowe and Palmer, 1995). A graphic implementation of one such model is shown in Figure 9. The dendritic arbor of a peripheral rabbit α cell is redrawn from Peichl et al. (1987). A mosaic of the axon terminal systems of a population of bipolar cells is also shown. The parameters of this population—density, coverage and regularity—were obtained from measurements of the population of calbindin bipolar cells (Massey and Mills, 1996). This is the leading candidate for providing the bipolar cell input to ON α cells in the rabbit. However, the fundamental analysis would be little influenced by choosing a different mosaic of bipolar cells—their size and axonal coverages are quite similar (Mills and Massey, 1992; Brown and Masland, 1999).

All bipolar cells whose axon terminals overlie the dendrites of the ganglion cell are considered to synapse on that ganglion cell (Freed and Sterling, 1988). They are marked in red (Figure 9A). The exception is that the soma and proximal dendrites do not receive bipolar cell input, as shown by previous anatomical studies (Kolb, 1979; Stevens et al., 1980; Freed and Sterling, 1988; Kolb and Nelson, 1993). This creates a relatively insensitive region over the soma and makes the regions of high sensitivity more distinct. It may help explain why, in our data, a region of low sensitivity was often located over the soma.

In Figure 9B, this input was blurred to mimic the lateral spread of the signal as it passes through the bipolar cells. In this example, we used a Gaussian function with twice the radius of the bipolar cell axon terminals to mimic the possible spread of neural activity (e.g., through coupling via gap junctions; Vaney, 1994; Mills and Massey, 1995). Although the exact amount of blur is unknown, this parameter can be widely varied and still produces the same qualitative result (data not shown). Without any blur, the sensitivity profiles are bumpier. To smooth the sensitivity profile, one must give the bipolar cells a receptive field four to five times their axonal arbor (150–200 μm), difficult to justify physiologically or anatomically. Similarly, varying the axonal coverage, size, or regularity can change the size and somewhat shift the location of the hot spots but does not change the fundamental result.

The resultant receptive field was sampled using the same stimulus size as the one used in our standard

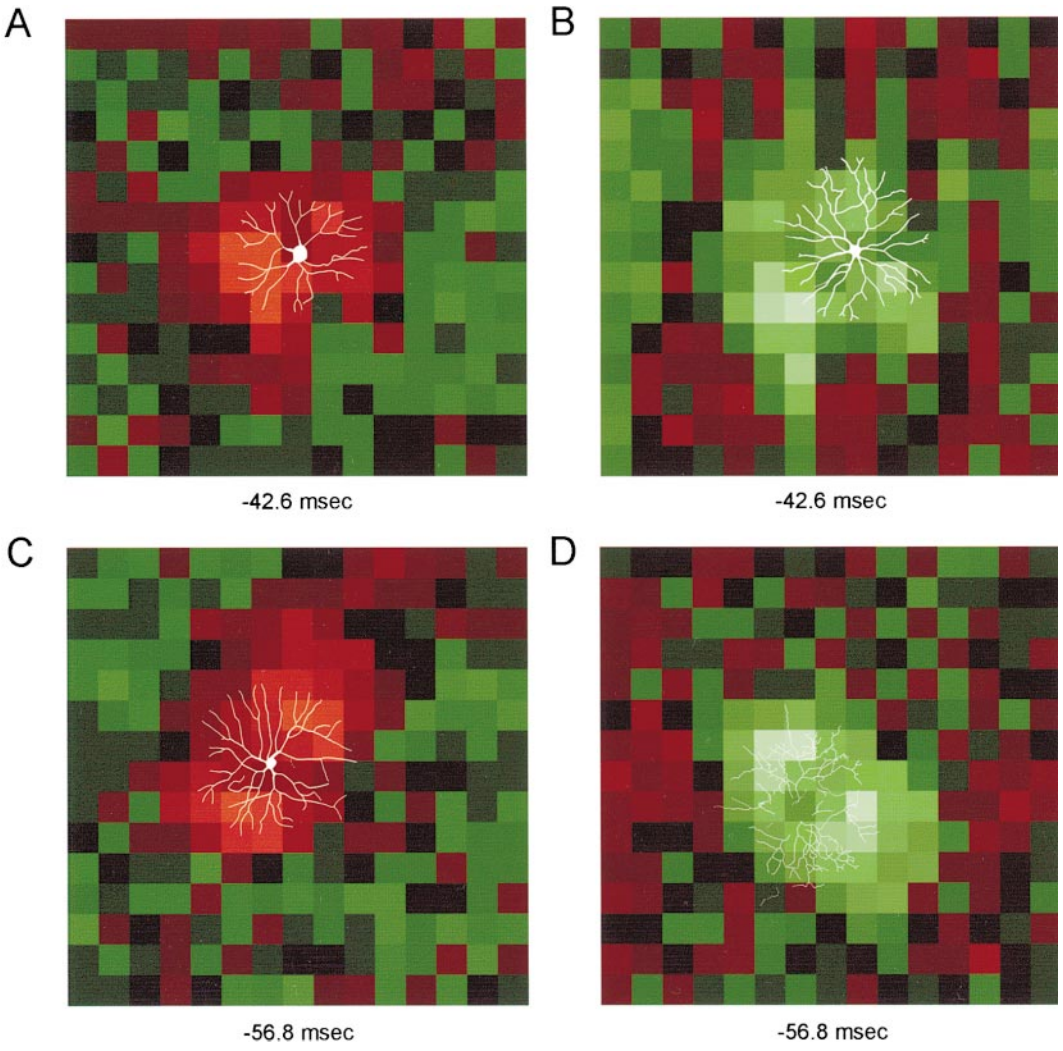


Figure 8. Four Examples of the Receptive Fields and Dendritic Fields from Two ON and Two OFF Retinal Ganglion Cells

Although the general outline of the receptive field was similar in most cases to the general outline of the dendritic field, the areas of high and low sensitivity did not obviously correlate with features within the dendritic arbor. Although the dendritic arbors are well filled, the distal tips of the largest cells may not be completely filled. For all four cells, the soma was located in a region of relatively decreased sensitivity in the receptive field. For example, the OFF cell in (C) had two regions of increased sensitivity within its receptive field center. Yet these regions did not have a dendritic density markedly different from the dendritic density of those areas of decreased sensitivity. Likewise, the ON cell in (B) had four regions of relatively high sensitivity surrounding the soma. Again, the relatively even distribution of dendrites in its symmetric dendritic field could not be used to predict which regions of the receptive field were most sensitive. Data from (B) were shown in Figure 6, data from (C) were shown in Figure 7A, and data from (D) were shown in Figure 5. Each square within the receptive field is 104 μm in width.

mapping protocol, 104 μm (Figure 9C). A small number of sensitive regions resulted within this receptive field, just as in the experimentally measured receptive fields. Note that the resulting receptive field map (Figure 9C) is not simply a blurred image of the dendritic arbor of the ganglion cell. Instead, it reflects the joint interaction of the bipolar cell mosaic, the paths of the ganglion cell's dendrites, and the matrix of test squares stimulated in a particular experiment.

Figure 9 thus attempts only a proof of principle—it shows how this three-way interaction can produce the kinds of inhomogeneity that we observed. Without knowledge of specific connectivity, its predictions for any individual cell are approximate. For greater precision, one would need experiments in which the receptive field, the arbor of the ganglion cell, and its connections with bipolar cells could simultaneously be studied. Two components of the analysis were available in a previous electron microscopic study, with a predicted result consistent with this model: anatomical jitter in bipolar input predicted an inhomogeneous profile of ganglion cell sensitivity (Freed et al., 1992). The ultimate experiment would probably require methods for identifying retinal synapses by confocal microscopy after labeling of a recorded ganglion cell by microinjection and its bipolar mosaic by immunohistochemistry.

### Uneven Sensitivity Profiles Represent Positional Uncertainty in the Signal Transmitted by Wide-Field Ganglion Cells to the Brain

In psychophysical experiments, rabbits can resolve stimuli subtending 10–20 min of arc, corresponding to 17–34 μm on the retina (van Hof, 1967). This may be

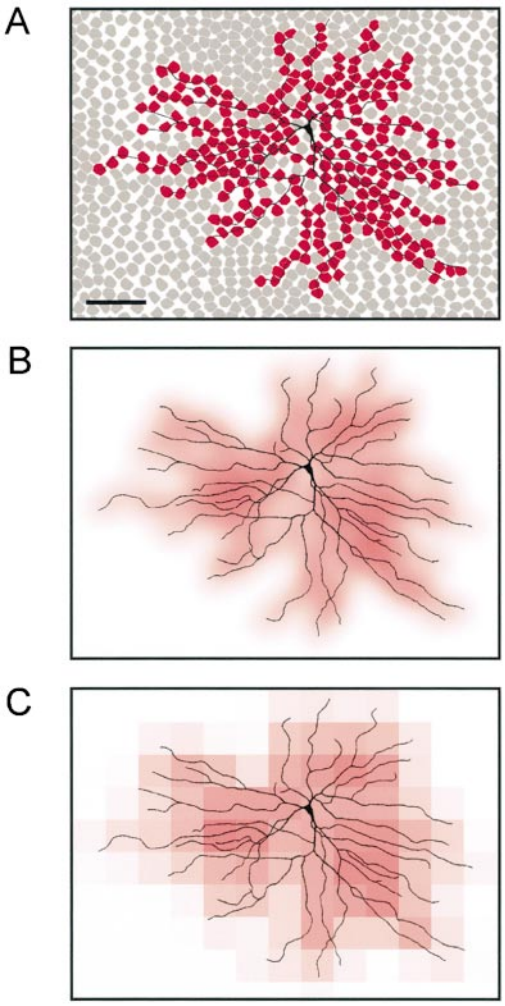


Figure 9. The Sampling of Bipolar Cell Axon Terminal Arbors by Dendrites of a Large Retinal Ganglion Cell

(A) An $\alpha$ cell from 11 mm eccentricity in the rabbit retina is shown (from Peichl et al., 1987a). A mosaic of axon terminals with a density of 566/mm$^2$ and a coverage of 0.67 replicates the characteristics of the population of calbindin bipolar cells at 11 mm eccentricity. Those bipolar cells whose axon terminal system contacts the dendrite of the $\alpha$ cell were marked in red. In accordance with anatomical data, the soma and the proximal dendrites (central 125 $\mu$m) receive no bipolar input. Scale bar, 200 $\mu$m.

(B) The image in (A) was blurred with a Gaussian filter two times the diameter of the axon terminal system of the bipolar cell. This was to take into account the lateral spread of activity in the retina, generated by gap junctions and other neural convergence and divergence. The irregularities in the sensitivity profile (shown below) persisted until a Gaussian four to five times the diameter of the bipolar cell axon terminal system was used.

(C) The sensitivity profile shown in (B) has been sampled with the pixel size (104 $\mu$m) used in our standard experiment, by averaging the intensity of the profile in (B) under each pixel. There are several regions of higher sensitivity located within this receptive field. Although their location varied, regions of high sensitivity were also seen when different bipolar cell mosaics were used.

compared with the scale of the observed receptive field microstructure, which spans hundreds of micrometers; the optics of the rabbit's eye would not smooth these variations. Just as quantal noise and synaptic noise introduce uncertainty about the intensity of a visual stimulus, irregular sensitivity across the ganglion cell's receptive field represents a form of spatial noise: uncertainty about stimulus position.

Why is this uncertainty greater for wide-field cells than for narrow-field, and what are its implications for central visual processing? The likely answer to the first question resides in the three-dimensional geometry of the cells' dendritic arbors and the concomitant differences in their inputs from bipolar cells. The axonal arbors of the various types of bipolar cells each ramify in different strata of the IPL (Boycott and Wässle, 1999). As a general rule, the dendritic arbors of narrow-field ganglion cells occupy several strata of the IPL, while wide-field cells are confined to a much narrower stratum (Wässle and Boycott, 1991; Linberg et al., 1996; Isayama et al., 2000). A narrow-field ganglion cell, such as the $\beta$ cell, receives synaptic input from several types of bipolar cells, each with an independent mosaic, while most of the arbor of the $\alpha$ cell receives input from only one (Freed and Sterling, 1988; Cohen and Sterling, 1992). The suggested reason for a ganglion cell to receive input from several types of bipolar cell is to expand its temporal bandwidth (Sterling et al., 1995; Boycott and Wässle, 1999). In the spatial domain, a consequence is that a narrow-field ganglion cell receives input from several overlapping mosaics of bipolar cells, while a wide-field cell may receive input from only a single mosaic (Figure 10).

While this makes the wide-field cell more vulnerable to the kind of distortion reported here, this arrangement is not unreasonable in light of the fates of their outputs within the central visual system. The $\beta$ cell and its homologs are used centrally for spatial vision—to detect high spatial frequencies under widely varying conditions of illumination. Wide-field cells, such as the $\alpha$ cell and the ON DS cell, detect change or motion on a larger scale (Levick, 1996; Vaney et al., 1999). For example, the receptive fields of many ON DS cells are combined centrally; neurons in the accessory optic system, which receive the output of the ON DS cells, have receptive fields much larger than those of the individual retinal ganglion cells and respond to global rather than local motion (Soodak and Simpson, 1988). Because the task of such systems is to survey movement over large areas, local irregularities in visual sensitivity would be of little consequence. Such an arrangement is an efficient adaptation to the bottleneck generated by the optic nerve because the visual scene can be surveyed using a relatively small number of ganglion cells (and also a small number of bipolar cells). Indeed, $\alpha$ cells represent $<5\%$ and ON DS cells $<1\%$ of all retinal ganglion cells in most mammalian retinas (Peichl et al., 1987b; Vaney et al., 1999).

#### Experimental Procedures

Extracellular recordings were performed essentially as previously described (Yang and Masland, 1992, 1994; Peters and Masland, 1996; He and Masland, 1997). Briefly, 1–4 days before the experiment, adult New Zealand white rabbits were anesthetized with ketamine (100 mg/kg) and xylazine (20 mg/kg). After application of a topical proparacaine solution (0.5%), either 10–20 $\mu$l of 1%–2% Fast blue (F-5756, Sigma, St. Louis, MO) was injected into one optic nerve via a small cut in the conjunctiva, or 10 $\mu$l of 0.05% 4,6 diamidino-2-phenolindole was injected intraocularly. The day of the experiment, the rabbit was dark adapted for several hours and then deeply anesthetized with ketamine (100 mg/kg) and xylazine (20

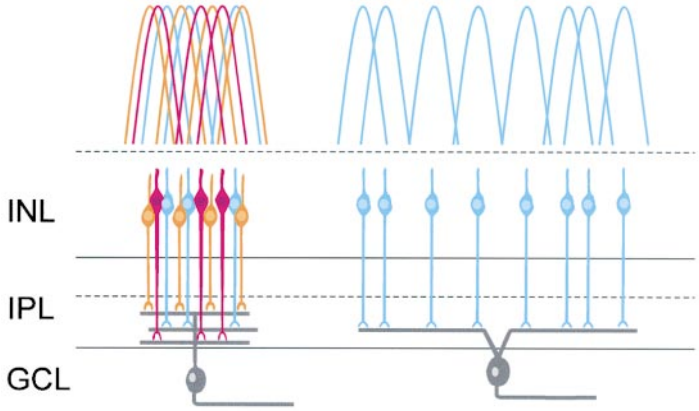


Figure 10. The Pattern of Bipolar Cell Input to Narrow-Field and Wide-Field Ganglion Cells

On the left, a narrow-field ganglion cell is illustrated, with a dendritic arbor spanning sublamina b of the IPL. On the right, a wide-field cell, with its narrowly stratifying dendritic arbor, is illustrated. The narrow-field cell samples the mosaics of several different bipolar cell types, while the wide-field cell receives its input predominantly from a single mosaic. The receptive field of the narrow-field cell results from the superposition of a number of overlapping bipolar cell receptive fields. The wide-field cell is much more vulnerable to the vagaries of the single bipolar cell mosaic that it samples. Abbreviations: INL, inner nuclear layer; IPL, inner plexiform layer; GCL, ganglion cell layer.

mg/kg) under dim red illumination. This anesthesia was supplemented with intraperitoneal urethane (1–2 g/kg) or topical proparacaine as needed. After enucleation, rabbits were euthanized with intravenous anesthetic in accordance with institutional guidelines. All protocols were approved by the Subcommittee on Research Animal Care of the Massachusetts General Hospital.

The retina was isolated in Ames medium (A-1420, Sigma) bubbled with $O_2/CO_2$ (95%:5%) as previously described (Ames and Nesbett, 1981; Yang and Masland, 1992). A small piece of retina was then removed and affixed photoreceptor-side down to a glass coverslip previously coated with 3–15 μl of Cell-Tak (40240, Collaborative Biomedical Products, Bedford, MA) and placed in the recording chamber mounted on a fluorescence microscope (Axioskop, Zeiss, Thornwood, NY). The preparation was superfused with oxygenated Ames medium at 35°C–37°C. Retinal ganglion cells were located by using brief pulses of fluorescent light, and cells with large somas in peripheral retina were preferentially targeted.

A total of 79 cells with concentric receptive fields was examined in this study. To lessen any systematic effects of a particular recording configuration, we used several different electrophysiological techniques. We recorded from 49 of these cells with tungsten electrodes (tungsten-in-glass [Levick, 1972] or 25–08–2, FHC, Brunswick, ME) or Ames-Pollen platinum–iridium electrodes (Ames and Pollen, 1969). The analog signal was amplified, filtered (MPA-20, Roveti, Annapolis, MD; 9002, Frequency Devices, Haverhill, MA), and digitized (Digidata-1200A and Axobasic, Axon Instruments, Foster City, CA). The remaining 30 cells were recorded using a loose seal cell-attached patch-clamp technique modified from Peters and Masland (1996). Briefly, glass electrodes whose tips were melted into 20–40 μm spheres and coated with poly-L-lysine (200–500 mg/ml, 150–300 kDa, P-1399, Sigma) were used to remove the Müller endfeet. The exposed area was then further cleaned using a vacuum pipette 20–40 μm in diameter. A borosilicate glass pipette (tip diameter of 2–8 μm, World Precision Instruments, Sarasota, FL) filled with extracellular solution recorded action potentials in the cell-attached mode. The analog signal was amplified, filtered (3900A, Dagan, Minneapolis, MN), and digitized as previously described. In all cases, action potentials were discriminated post hoc, prior to further analyses.

Visual stimuli were projected with a computer monitor (Dell Trinitron, Austin, TX; 449Xa, Nokia, Sausalito, CA) and reflected, via a substage mirror, through a 20× objective (LD Achroplan NA 0.4, Zeiss; LCPlanFl NA 0.4, Olympus), which replaced the microscope's condenser. The light therefore entered the retina from the photoreceptor side, while the electrode approached the retina from the ganglion cell side; this configuration eliminated shadows cast by the electrode within the receptive field. Once the tissue had been placed in the perfusion chamber, the image of the monitor was focused by projecting a test square onto the preparation and adjusting the substage objective until the square was sharply in focus.

The stimulus was a flickering checkerboard composed of 15 × 15 squares; the luminance of each square was independently modulated every 14.2 ms (one frame at ~70 Hz) or occasionally every 28.4 ms. The width of the squares in the checkerboard was varied from 32 to 104 μm (~0.2° to 0.6° of visual angle).

We used two different techniques to generate the pseudorandom sequences used to modulate the luminances of the stimulus pixels: a multiplicative linear congruential random number generator (Park and Miller, 1988) and M sequences (Sutter, 1992; Reid et al., 1997). Interactions between the response nonlinearities of the cell under study and the statistics of a particular pseudorandom sequence can distort the spike-triggered stimulus average in different ways. As an additional control, we used the inverse repeat method of Sutter to map the cells (Sutter, 1992). The polarity of the M sequence was reversed and used to map the cell a second time. By averaging the receptive field maps generated by the two stimulus polarities, the contribution from second- and higher-order even nonlinearities was eliminated from the spike-triggered stimulus average. In no case did changing the pseudorandom sequence qualitatively change the sensitivity profile of the cells we tested ($n = 7$).

Previous experiments found no difference between receptive field maps of cat ganglion cells obtained using a spatiotemporal white noise stimulus and a conventional serial presentation of spots (Citron et al., 1988), and we confirmed these findings in a subset of the cells ($n = 4$). After computing the spatiotemporal receptive field, we mapped the receptive field of the cell by presenting each 104 μm spot of light for 200 ms followed by 1.5 s of dim background at each position in the 15 × 15 array. The order of the 225 spot presentations was randomly interleaved within each of the ten repetitions.

The receptive fields of 25 ON–OFF DS ganglion cells and 2 ON DS ganglion cells were also analyzed. These cells were identified by their directional response to a light bar moving along its long axis for 12 different orientations (every 30°). Stimuli were generated using a CRT image synthesizer (Innisfree, Cambridge, MA) controlled via computer and displayed on a Tektronics 608 monitor. The action potentials were recorded using conventional techniques.

The monitors were calibrated with an LS-100 luminance meter (Minolta, Ramsey, NJ), and their nonlinear input–output function was corrected in software with a look-up table. A photodiode (S1133–12, Hammamatsu, Middlesex, NJ) mounted on the microscope stage was used to calibrate the stimulus luminance at the position of the preparation. The stimuli ranged in intensity from 0 to 10 cd/m$^2$.

We developed software in-house to determine each neuron's spatiotemporal receptive field by calculating the spike-triggered stimulus average for the cell (De Boer and Kuyper, 1968; Mizuno et al., 1985). The action potentials were binned at the stimulus refresh rate, typically 14.2 ms. When the response to more than one 7–15 min stimulus run was recorded, the receptive fields were averaged together, unless otherwise noted.

For the cells in our sample, the same pixels within the spatiotemporal spike-triggered stimulus average were consistently the most influential, even at different time points—or phases (ON or OFF)—of the response. We therefore defined the receptive field as the stimulus frame with the maximum modulation of the sign of the cell's response to a single spot. This latter criterion was used because, for some cells, the strongest modulation was of the polarity opposite

of the cell's response to a single spot. In other words, for an ON cell whose preferred stimulus was an OFF-to-ON transition, the maximum modulation might be in the OFF phase of the spike-triggered average. In some figures, the receptive field was thresholded, so that only those pixels modulated more than three standard deviations from the mean are shown. The center of mass of the receptive fields was calculated from the stimulus-normalized intensities of the unthresholded spatial receptive field.

The autocorrelogram was calculated for each recording using a bin width of 0.1 ms and was normalized by the total number of action potentials. These autocorrelograms were used to confirm that the action potentials originated from a single cell; recordings with autocorrelograms that lacked an absolute refractory period were excluded.

After the recording session, the ganglion cell was injected with 4% Lucifer yellow as previously described (Yang and Masland, 1992, 1994; He and Masland, 1997). During the injection, great care was taken to ensure that the soma did not move relative to the stimulus. If the cell moved, it was eliminated from the analysis. To ensure that the receptive field and the dendritic field were correctly aligned, the cell body and proximal dendrites were immediately photographed at relatively high magnification (40× Achroplan NA 0.75, Zeiss) with a fiduciary mark projected from the stimulus monitor. The cell was then further photographed at lower magnification to capture the entire dendritic tree.

The tissue was then fixed at 4°C for 1 hr in 4% paraformaldehyde (Ted Pella, Redding, CA) or overnight in 2% paraformaldehyde. Some injected cells were processed with immunochemistry to convert the Lucifer yellow to a permanent reaction product. The tissue was incubated overnight in 0.5% Triton X-100 and 4% normal goat serum. The tissue was then incubated for 3 days in the same solution with biotinylated anti-Lucifer yellow (1:200; A-5750, Molecular Probes, Eugene, OR) followed by 1 day in ABC solution (Vectastain Elite ABC Kit, Vector Laboratory, Burlingame, CA). Diaminobenzidine (Kirkegaard and Perry Laboratories, Gaithersburg, MD) was used to visualize the staining.

## Acknowledgments

This work was supported by a Howard Hughes Medical Institute Predoctoral Fellowship to S. P. B. R. H. M. is a Senior Investigator of Research to Prevent Blindness. We thank T. Euler for helpful discussions, R. Rockhill for technical assistance, and L. Peichl for the use of the cell in Figure 9.

Received February 22, 2000; revised June 19, 2000.

## References

Ames, A., and Nesbett, F.B. (1981). *In vitro* retina as an experimental model of the central nervous system. J. Neurochem. *37*, 867–877.

Ames, A., and Pollen, D.A. (1969). Neurotransmission in central nervous tissue: a study of isolated rabbit retina. J. Neurophysiol. *32*, 424–442.

Boycott, B., and Wässle, H. (1999). Parallel processing in the mammalian retina. Invest. Ophthalmol. Vis. Sci. *40*, 1313–1327.

Brown, S.P., and Masland, R. (1999). Costratification of a population of bipolar cells with the direction-selective circuitry of the rabbit retina. J. Comp. Neurol. *408*, 97–106.

Chichilnisky, E.J., and Baylor, D.A. (1999). Receptive-field microstructure of blue-yellow ganglion cells in primate retina. Nat. Neurosci. *2*, 889–893.

Citron, M.C., Emerson, R.C., and Levick, W.R. (1988). Nonlinear measurement and classification of receptive fields in cat retinal ganglion cells. Ann. Biomed. Eng. *16*, 65–77.

Cohen, E., and Sterling, P. (1991). Microcircuitry related to the receptive field center of the ON-beta ganglion cell. J. Neurophysiol. *65*, 352–359.

Cohen, E., and Sterling, P. (1992). Parallel circuits from cones to the ON-beta ganglion cell. Eur. J. Neurosci. *4*, 506–520.

Creutzfeldt, O.D., Sakmann, B., Scheich, H., and Korn, A. (1970). Sensitivity distribution and spatial summation within receptive-field center of retinal on-center ganglion cells and transfer function of the retina. J. Neurophysiol. *33*, 654–671.

Dawis, S., Shapley, R., Kaplan, E., and Tranchina, D. (1984). The receptive field organization of X-cells in the cat: spatiotemporal coupling and asymmetry. Vision Res. *24*, 549–564.

De Boer, E., and Kuyper, P. (1968). Trigger correlation. IEEE Trans. Biomed. Eng. *15*, 169–179.

Derrington, A.M., and Lennie, P. (1982). The influence of temporal frequency and adaptation level on receptive field organization of retinal ganglion cells in cat. J. Physiol. *333*, 343–366.

DeVries, S.H., and Baylor, D.A. (1997). Mosaic arrangment of ganglion cell receptive fields in rabbit retina. J. Neurophysiol. *78*, 2048–2060.

Enroth-Cugell, C., and Freeman, A.W. (1987). The receptive-field structure of cat retinal Y cells. J. Physiol. *384*, 49–79.

Enroth-Cugell, C., and Robson, J.G. (1966). The contrast sensitivity of retinal ganglion cells of the cat. J. Physiol. *187*, 517–552.

Enroth-Cugell, C., Robson, J.G., Schweitzer, D.E., and Watson, A.B. (1983). Spatio–temporal interactions in cat retinal ganglion cells showing linear spatial summation. J. Physiol. *341*, 279–307.

Freed, M.A., and Sterling, P. (1988). The ON-alpha ganglion cell of the cat retina and its presynaptic cell types. J. Neurosci. *8*, 2303–2320.

Freed, M.A., Smith, R.G., and Sterling, P. (1992). Computational model of the on-alpha ganglion cell receptive field based on bipolar cell circuitry. Proc. Natl. Acad. Sci. USA *89*, 236–240.

Hawken, M.J., and Parker, A.J. (1987). Spatial properties of neurons in the monkey striate cortex. Proc. R. Soc. Lond. B Biol. Sci. *231*, 251–288.

He, S., and Masland, R.H. (1997). Retinal direction selectivity after targeted laser ablation of starburst amacrine cells. Nature *389*, 378–382.

Hochstein, S., and Shapley, R.M. (1976). Linear and non-linear spatial subunits in Y cat retinal ganglion cells. J. Physiol. *262*, 265–284.

Isayama, T., Berson, D.M., and Pu, M. (2000). Theta ganglion cell type of cat retina. J. Comp. Neurol. *417*, 32–48.

Kier, C.K., Buchsbaum, G., and Sterling, P. (1995). How retinal microcircuits scale for ganglion cells of different size. J. Neurosci. *15*, 7673–7683.

Koch, C., Poggio, T., and Torre, V. (1982). Retinal ganglion cells: a functional interpretation of dendritic morphology. Philos. Trans. R. Soc. Lond. B Biol. Sci. *298*, 227–264.

Kolb, H. (1979). The inner plexiform layer in the retina of the cat: electron microscopic observations. J. Neurocytol. *8*, 295–329.

Kolb, H., and Nelson, R. (1993). OFF-alpha and OFF-beta ganglion cells in cat retina: II. Neural circuitry as revealed by electron microscopy of HRP stains. J. Comp. Neurol. *329*, 85–110.

Levick, W. (1996). Receptive fields of cat retinal ganglion cells with special reference to the *alpha* cells. Prog. Ret. Eye Res. *15*, 457–500.

Levick, W.R. (1972). Another tungsten microelectrode. Med. Biol. Eng. *10*, 510–515.

Linberg, K.A., Suemune, S., and Fisher, S.K. (1996). Retinal neurons of the California ground squirrel, *Spermophilus beecheyi*: a Golgi study. J. Comp. Neurol. *365*, 173–216.

Linsenmeier, R.A., Frishman, L.J., Jakiela, H.G., and Enroth-Cugell, C. (1982). Receptive field properties of X and Y cells in the cat retina derived from contrast sensitivity measurements. Vision Res. *22*, 1173–1183.

Massey, S.C., and Mills, S.L. (1996). A calbindin-immunoreactive cone bipolar cell type in the rabbit retina. J. Comp. Neurol. *366*, 15–33.

Mills, S.L., and Massey, S.C. (1992). Morphology of bipolar cells labeled by DAPI in the rabbit retina. J. Comp. Neurol. *321*, 133–149.

Mills, S.L., and Massey, S.C. (1995). Differential properties of two gap junctional pathways made by AII amacrine cells. Nature *377*, 734–737.

Mizuno, M., Imai, S., Tsukada, M., Hida, E., and Naka, K.-I. (1985).

A micro-computer system for spatio–temporal visual receptive field analysis. IEEE Trans. Biomed. Eng. *32*, 56–59.

Park, S.K., and Miller, K.W. (1988). Random number generators: good ones are hard to find. Communications ACM *31*, 1192–1201.

Peichl, L., Buhl, E.H., and Boycott, B.B. (1987a). Alpha ganglion cells in the rabbit retina. J. Comp. Neurol. *263*, 25–41.

Peichl, L., Ott, H., and Boycott, B.B. (1987b). Alpha ganglion cells in mammalian retinae. Proc. R. Soc. Lond. B Biol. Sci. *231*, 169–197.

Peters, B.N., and Masland, R.H. (1996). Responses to light of starburst amacrine cells. J. Neurophysiol. *75*, 469–480.

Reid, R.C., Victor, J.D., and Shapley, R.M. (1997). The use of m-sequences in the analysis of visual neurons: linear receptive field properties. Vis. Neurosci. *14*, 1015–1027.

Rodieck, R.W. (1965). Quantitative analysis of cat retinal ganglion cell response to visual stimuli. Vision Res. *5*, 583–601.

Rowe, M.H., and Cox, J.F. (1993). Spatial receptive-field structure of cat retinal W cells. Vis. Neurosci. *10*, 765–779.

Rowe, M.H., and Palmer, L.A. (1995). Spatio–temporal receptive-field structure of phasic W cells in the cat retina. Vis. Neurosci. *12*, 117–139.

Soodak, R.E. (1986). Two-dimensional modeling of visual receptive fields using Gaussian subunits. Proc. Natl. Acad. Sci. USA *83*, 9259–9263.

Soodak, R.E., and Simpson, J.I. (1988). The accessory optic system of rabbit. I. Basic visual response properties. J. Neurophys. *60*, 2037–2054.

Soodak, R.E., Shapley, R.M., and Kaplan, E. (1991). Fine structure of receptive-field centers of X and Y cells of the cat. Vis. Neurosci. *6*, 621–628.

Sterling, P., Smith, R.G., Rao, R., and Vardi, N. (1995). Functional architecture of the mammalian outer retina and bipolar cells. In Neurobiology and Clinical Aspects of the Outer Retina, M. Djamgoz et al., eds. (London, UK: Chapman and Hall), pp. 325–348.

Stevens, J.K., McGuire, B.A., and Sterling, P. (1980). Toward a functional architecture of the retina: serial reconstruction of adjacent ganglion cells. Science *207*, 317–319.

Sutter, E.E. (1992). A deterministic approach to nonlinear systems analysis. In Nonlinear Vision: Determination of Neural Receptive Fields, Function and Networks, R.B. Pinter and B. Nabet, eds. (Boca Raton, FL: CRC Press), pp. 171–220.

Thibos, L.N., and Levick, W.R. (1983). Bimodal receptive fields of cat retinal ganglion cells. Vision Res. *23*, 1561–1572.

van Hof, M.W. (1967). Visual acuity in the rabbit. Vision Res. *7*, 749–751.

Vaney, D.I. (1994). Patterns of neuronal coupling in the retina. Prog. Ret. Eye Res. *13*, 301–355.

Vaney, D.I., He, S., Taylor, W.R., and Levick, W.R. (1999). Direction-selective ganglion cells in the retina. In Processing Visual Motion in the Real World, J. Zanker and J. Zeil, eds. (Berlin: Springer-Verlag).

Velte, T.J., and Miller, R.F. (1995). Dendritic integration in ganglion cells of the mudpuppy retina. Vis. Neurosci. *12*, 165–175.

Wässle, H., and Boycott, B.B. (1991). Functional architecture of the mammalian retina. Physiol. Rev. *71*, 447–480.

Yang, G., and Masland, R.H. (1992). Direct visualization of the dendritic and receptive fields of directionally selective retinal ganglion cells. Science *258*, 1949–1952.

Yang, G., and Masland, R.H. (1994). Receptive fields and dendritic structure of directionally selective retinal ganglion cells. J. Neurosci. *14*, 5267–5280.